AIP Advances

Dynamical properties and their strain-dependence of ZnSe(ZnSe:N): Zinc-blende and wurtzite

Dandan Wang, Xiaojun Zhang, Binghui Li, Lei Liu, and D. Z. Shen

Citation: AIP Advances **4**, 067138 (2014); doi: 10.1063/1.4885466
View online: http://dx.doi.org/10.1063/1.4885466
View Table of Contents: http://scitation.aip.org/content/aip/journal/adva/4/6?ver=pdfcov
Published by the AIP Publishing

AIP ADVANCES **4**, 067138 (2014)

Dynamical properties and their strain-dependence of ZnSe(ZnSe:N): Zinc-blende and wurtzite

Dandan Wang,[1,2] Xiaojun Zhang,[3,4] Binghui Li,[5,a] Lei Liu,[5,b] and D. Z. Shen[5]
[1]*State Key Laboratory of Luminescence and Applications, Changchun Institute of Optics, Fine Mechanics and Physics, Chinese Academy of Sciences, No.3888 Dongnanhu Road, Changchun, 130033, People's Republic of China*
[2]*University of Chinese academy of sciences, Beijing 100039, People's Republic of China*
[3]*Lawrence Berkeley National Laboratory, Berkeley, California 94720, USA*
[4]*Department of Mechanical Engineering, University of California at Berkeley, Berkeley, California 94720, USA*
[5]*State Key Laboratory of Luminescence and Applications, Changchun Institute of Optics, Fine Mechanics and Physics, Chinese Academy of Sciences, No.3888 Dongnanhu Road, Changchun, 130033, People's Republic of China*

(Received 16 April 2014; accepted 12 June 2014; published online 24 June 2014)

The lattice dynamical properties of ZnSe and ZnSe with substitutional N incorporation(ZnSe:N) are investigated in both the zinc-blend(ZB) and wurtzite(WZ) structures using first-principles calculations. The optical phonon modes of ZB-ZnSe at the Γ-point locate at 250 cm^{-1} for LO and 213 cm^{-1} for TO. The characteristic E_2 phonon modes at about 50 cm^{-1} and the E_1 and another E_2 phonon modes around 200 cm^{-1} of WZ-ZnSe are suggested to be the fingerprint for distinguishing the two polytypes of ZnSe. For substitutional N incorporated ZnSe, the N incorporation introduces three new high energy modes above 500 cm^{-1}, and the splitting of them is much larger in the WZ phase than that in ZB phase. The strain dependence of phonon frequency which could be useful for corresponding spectroscopic strain characterization are also studied. The simple linear dependence is determined for ZB-ZnSe, while the situation for WZ-ZnSe looks more complicated. [http://dx.doi.org/10.1063/1.4885466]

I. INTRODUCTION

Zinc selenium(ZnSe), a fundamental group II-VI semiconductor with a direct band gap of 2.70 eV at room temperature,[1] has been extensively studied as a potential material for light-emitting diodes in blue region and other photoelectric devices.[2–5] Characterized by their sp^3 bonding, the ZnSe crystals have two common structure polytypes, namely zinc-blend and wurtzite, like other sp^3 covalent-bond semiconductors. Since the ZB and WZ structures differ only in the third-nearest-neighbor atomic arrangement, their electronic properties behave rather similarly. Both ZnSe phases possess almost the same bandgap (E_g), with a difference of only 0.05 eV ($E_g^{WZ} > E_g^{ZB}$).[6] The optical phonons which are sensitive to the crystallographic difference between ZB and WZ structures can be used to distinguish the ZnSe phases from each other. Hennion *et al*. have measured the phonon dispersion curves of ZnSe at room temperature using the inelastic neutron scattering.[7] Cerdeira *et al*. have reported the measurement of the frequency of the Γ optical phonons in ZnSe and the effects of large static uniaxial stress on those phonons employing first-order Raman scattering.[8] Several first-principles calculations have also been performed to study the dynamical properties of ZnSe.[9–11] However, although so far there have several reports on the phonon dispersion of ZnSe, few

[a]Electronic mail: luminescence@ciomp.ac.cn
[b]Electronic mail: liulei@ciomp.ac.cn

of them describe the WZ phonons. One of the main aims of this work is to provide a thorough DFPT investigation of the vibrational properties of ZnSe in both phases. The phonon dispersion curves of ZB-ZnSe obtained in this work possess essential accuracy with the data available in the literature.[7–9]

The second aim in our work is to illuminate the vibrational properties of N doped ZnSe. The *p*-type ZnSe doped with nitrogen has been under focus for decades due to the essential of *p*-*n* junctions for light-emitting devices.[12,14] It was found experimentally that even the nitrogen doping may induce the WZ phase of ZnSe.[13] The N is generally supposed to incorporate on Se substitutional site and its introduction would change the bond distances and lower the symmetry in the crystal system. Consequently, the phonon modes will be altered and new optical phonons will be introduced. What's more, due to the different chemical environment around the substitutional N in ZB- and WZ-ZnSe, the new optical phonons introduced by N incorporation differ in those two phases. The phonon features of ZnSe with substitutional N incorporation(ZnSe:N) in ZB and WZ phases need to be clarified.

For the real application of light-emitting devices, ZnSe crystals are usually grown on foreign substrates by molecular beam epitaxy (MBE) or metal organic vapor phase epitaxy (MOVPE) techniques. The lattice mismatch and different thermal expansion coefficients between epitaxial layers and substrates inevitably lead to the presence of built-in strains in the hetero-layers. For example, Nakashima *et al*. have observed using Raman spectroscopy the variation of the ZnSe LO phonon frequency with thickness due to the elastic strains in ZnSe films grown by MBE on GaAs and evaluated strains in ZnSe films.[15] What's more, from a crystallography point of view, the low-symmetry WZ structure contains only one primary glide plane, i.e. the (0001) plane, while its cubic counterpart have more glide planes, mainly the $\{111\}$ glide sets.[16,17] Due to such lowered translational symmetry, the interfacial dislocations extension can be suppressed in the WZ type epilayers grown on substrates. Therefore, it has been suggested that the lifetime of light-emitting devices especially the laser diodes may be improved by replacing the normally cubic-structured active layer with a hexagonal one.[18,19] However, under normal conditions the as-grown bulk ZnSe exists in the ZB phase. WZ-ZnSe materials are usually prepared in low dimensional nano-scale.[20–22] The size confinement and surface effect will also lead to built-in strain in nanostructure. Since strain can impact generally the structural, electrical, and optical properties of semiconductors, its characterization would also be meaningful for ZnSe in designing and optimizing its optoelectronic devices. Saib *et al*. have proved that both LO and TO phonon frequencies of zinc-blende ZnSe at zone center showed an increase with rising pressure based on the density functional perturbation theory.[24] As the collective lattice vibrations, phonon that responds to lattice distortion can be taken as an efficient way for the strain measurement in semiconductors. We have deduced the strain distribution in the semiconductor materials based on the dependence of phonon frequencies versus hydrostatic pressure.[25] So the third aim of our work is to investigate the strain dependence of the optical phonon frequencies at the Γ point of ZnSe in both ZB and WZ phases, which can be regarded as guide to determine the strain distribution in ZnSe.

II. THEORETICAL DETAILS

In this paper, the vibrational properties are calculated employing density-functional perturbation theory(DFPT).[26] The DFPT calculations are performed based on Perdew-Burke-Ernzerhof (PBE) generalized gradient approximation[27] and the projected augmented wave (PAW) method using the Vienna *ab initio* simulation package (VASP).[28–31] To extract the force constants and generate the phonon spectra, the PHONONPY code is employed. Following the PBE results, we have the theoretical lattice parameters of ZB and WZ phases of ZnSe: a_{ZB}=5.74 Å, a_{WZ}=b_{WZ}=4.05 Å, c_{WZ}=6.61 Å. These theoretical lattice parameters are larger than experimental values:[23] a_{ZB}=5.65 Å, a_{WZ}=b_{WZ}=4.00 Å, c_{WZ}=6.52 Å, as PBE normally overestimate the lattice parameters. By altering the lattice constants, the strain is introduced into the model structures where the atomic positions are relaxed until their residual forces are $< 0.01\ eV \cdot$ Å $^{-1}$. In all calculations, a plane-wave basis set with 400 eV cutoff is used to expand the electronic wave functions and the Brillouin zone is sampled with the kpoint separation < 0.04 Å $^{-1}$.

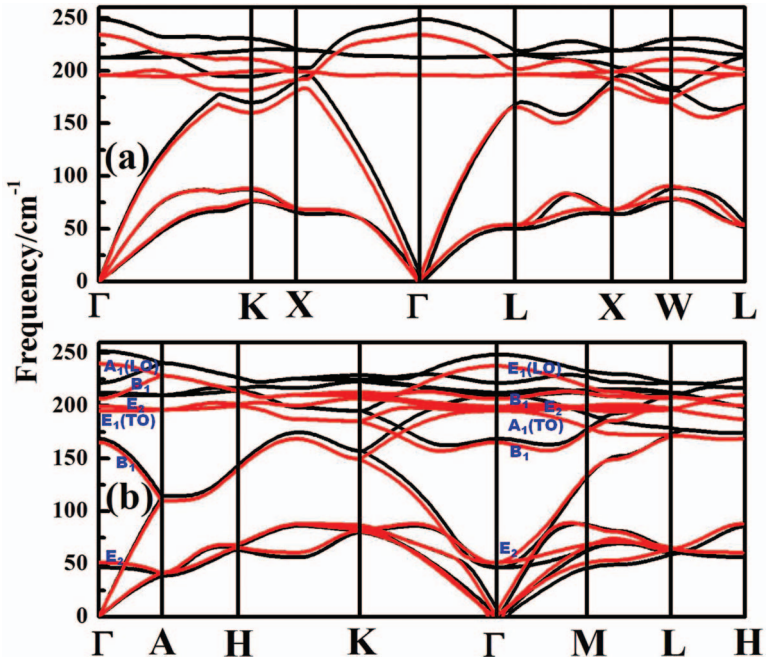

FIG. 1. Calculated phonon dispersion curves for bulk ZnSe in (a) zinc-blend structure and (b) wurtzite structure. Where the black curves represent the phonon dispersion curves based on the experimental lattice constants, and those red ones are from the model of theoretical lattice constants.

III. RESULTS AND DISCUSSIONS

A. Phonon dispersion curves of ZB and WZ-ZnSe

The calculated phonon dispersion curves along the high symmetry directions of ZB-ZnSe are plotted in Fig. 1(a). Those curves based on the experimental lattice parameters are plotted in the black lines, and those based on the theoretical ones are in the red lines. With two atoms per unit cell, the ZB phonons have three acoustic phonon modes and three optical ones. The calculated phonon dispersion curves agree well with the experimentally obtained results.[7] In comparison with the existing experimental critical point phonon frequencies (in cm^{-1}, Γ: 213, 253; X: 70, 194, 213, 219; L : 57, 166, (to be verified: 234)) measured by neutron scattering,[7] the calculated ZB phonon dispersion curves on experimental constant of a_{ZB}=5.65 Å give the better agreement with the values (in cm^{-1}, Γ: 212, 249; X: 64, 195, 203, 219; L : 57, 170, 215, 218.). In comparison with other results, the frequencies of optical phonons at the Brillouin zone center are listed in Table I, together with Born charges. At Γ, the degeneracy of the optical modes is removed, bringing about LO-TO splitting. This LO-TO splitting originates from the long-range Coulomb interactions which can be described by Born effective charge tensors.[32] In the cubic structure, the Born effective charge tensors $Z_{Zn}{}^*$ and $Z_{Se}{}^*$ are both diagonal with only one distinct component due to high symmetry. Based on Fig. 1(a), the phonon modes for ZB-ZnSe from the theoretical parameters, especially those optical ones, are consequently with lower frequencies compared with those from the experimental parameters. This behavior can be explained by , equivalently, the tensile strain in theoretical crystal due to about 1.6% larger lattice constants compared to experimental crystal. It prove that phonon modes are sensitive to strain fields. And the dependence of optical phonon frequencies at Γ on strain for ZnSe will be discussed in detail later.

In Fig. 1(b), we show two sets of calculated phonon dispersion curves for WZ-ZnSe, one for theoretical lattice parameters and the other for experimental ones. Similar to the ZB case, the optical phonon modes on experimental lattice parameter are higher than those obtained by theoretical lattice parameter. Moreover, the phonon modes of WZ-ZnSe are more complex since with more atoms in the primitive cell. WZ-ZnSe possess nine optical modes, as: $A_1+2B_1+E_1+2E_2$. Among them, E_1

TABLE I. Optical phonon frequencies (in cm^{-1}) at Γ, and the distinct tensor components of Born effective charge for ZnSe in ZB and WZ structure. Based on space group theory, the A_1, $2B_1$, E_1 and $2E_2$ phonons in the WZ structure respectively have the symmetries : Γ_1, Γ_3, Γ_5 and Γ_6. For optical Γ-phonon frequencies obtained in present work, the values before / are for theoretical lattice constants and those after / for experimental lattice constants.

	Present work	Other DFPT	Experiment
Zinc-blend			
LO	233.98/249.11	253.10[9]	253.00,[7] 252[33]
TO	195.56/212.61	211.18[9]	213.00,[7] 205[33]
$Z_{Zn}{}^*$	2.12/2.04	–	–
$Z_{Se}{}^*$	−2.17/−2.08	–	–
Wurtzite			
A_1	239.62/251.52	–	–
E_1	237.73/249.12	–	–
B_1	206.47/221.46	–	–
E_2	199.11/212.10	–	–
E_1	194.81/209.71	–	–
A_1	194.51/209.12	–	–
B_1	165.03/168.47	–	–
E_2	51.16/46.41	–	–
$Z(Zn)_{xx}{}^*$	2.03/1.97	–	–
$Z(Zn)_{zz}{}^*$	2.13/2.07	–	–
$Z(Se)_{xx}{}^*$	−2.04/−1.97	–	–
$Z(Se)_{zz}{}^*$	−2.14/−2.07	–	–

and the two E_2 modes are double degenerate. Based on group theory, it's expected that the A_1 and E_1 modes are both Raman and infrared active, the E_2 modes are Raman active only, and the B_1 ones are silent. The calculated optical phonon frequencies at the Γ point of these modes are also listed in Table I. At K points away from the zone center, such as along Γ → A (parallel to the c-axis) and Γ → M (perpendicular to the c-axis), the LO and LO modes can be distinguished as shown in Fig. 1(b). For convenience and picture clearness, only the point group labels for phonons of theoretical lattice constants are marked out by blue characters and their sequence is the same for those of experimental lattice constants. The splitting between the A_1(LO) and A_1(TO) created by the Born charge is larger than the splitting between E_1(LO) and E_1(TO) created by the lowering of the crystal symmetry. The A_1(LO)-A_1(TO) splitting is 42.40 cm^{-1} based on experimental lattice constants and 45.11 cm^{-1} on theoretical lattice constants, while the corresponding E_1(LO)-E_1(TO) splitting are respectively 39.41 cm^{-1} and 42.92 cm^{-1}. As seen in Table I, $Z_{Zn}{}^*$ and $Z_{Se}{}^*$ are also diagonal with two distinct components $Z_{xx}{}^*$ and $Z_{zz}{}^*$ in WZ-ZnSe, providing bigger LO-TO splitting value than that in ZB-ZnSe. In experimental spectroscopic measurements, the appearance of E_2 modes at about 50 cm^{-1} can be used to characterize WZ-ZnSe. In addition, in comparison with the ZB TO modes, WZ-ZnSe presents the E_1 and E_2 vibrations with the similar energy that may show the broader Raman features with peak splitting.

B. Phonon features of ZnSe:N

To study the phonon features of ZnSe with substitutional N incorporation (ZnSe:N) in ZB and WZ phases, a 64-atom supercell is selected for modelling its ZB structure, and a 72-atom supercell is used for its WZ structure. The calculated ZnSe phonon dispersion curves with N at the Se site (N_{Se}) are presented in Fig. 2. Similar as in the bulk case, the optical phonon frequencies based on the experimental lattice parameters are higher than those of theoretical ones. For ZB-ZnSe:N, three high new modes belonging to the alien N atoms appear above the 500 cm^{-1}. The highest LO phonon frequency in Fig. 2(a) is 29.1 cm^{-1} lower than the LO mode of 547.4 cm^{-1} in Fig. 2(b). It is meaningful to note that if a defect complex of N_{Se}-Se_{Zn} formed in the ZB ZnSe, a even higher LO phonon mode at the Γ point will be introduced, whose value can be around 596 cm^{-1} in the supercell based on the experimental lattice constants. In both Fig. 2(a) and Fig. 2(b), two

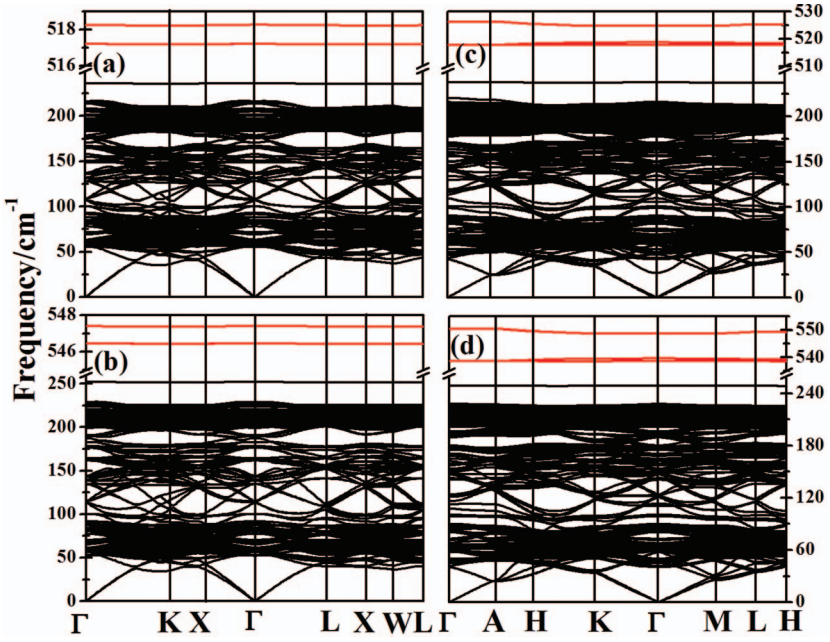

FIG. 2. Calculated phonon dispersion curves for substitutional N-doped ZnSe in (a) ZB structure based on theoretical lattice parameters; (b) ZB structure based on experimental lattice parameters; (c) WZ structure with theoretical lattice parameters; (d) WZ structure with experimental lattice parameters.

TO modes of N stay about 1 cm^{-1} below the LO mode at Γ point. In addition, the Born effective charge tensor of N $Z(N)^*$ is isotropic and the value of its instinct component is almost the same as its nominal value. However, new distinct components appear for $Z(Zn)^*$ and $Z(Se)^*$ because the alien N breaks the lattice symmetry and changes the chemical environment of them. Take the four nearest neighbor Zn atoms of the N atom as an example, the diagonal element of $Z(Zn)^*$ is about 2.40 and three new non-diagonal elements arise, namely $Z(Zn)_{xy}{}^*$ ($=Z(Zn)_{yx}{}^*$), $Z(Zn)_{xz}{}^*$ ($=Z(Zn)_{zx}{}^*$), $Z(Zn)_{yz}{}^*$ ($=Z(Zn)_{zy}{}^*$), with the absolute values of about 0.28.

For WZ-ZnSe:N, there are also three new modes belonging to N as shown in Fig. 2(c) and Fig. 2(d). But, the energy difference between the high-frequency LO mode and the two degenerate TO modes is much bigger than that in the ZB case. At the Γ point, frequencies of these N modes are 526.3 cm^{-1} and 517.8 cm^{-1} in Fig. 2(c), while they are 550.3 cm^{-1} and 538.6 cm^{-1} in Fig. 2(d). This bigger splitting of N modes in WZ-ZnSe:N than that in ZB-ZnSe:N may originates from the polarity of the WZ crystal. In addition, a stronger dynamic charge transfer also occurs in WZ-ZnSe:N than in ZB-ZnSe:N. Take the supercell model based on the theoretical lattice parameters as an example, the two distinct components of $Z(N)^*$ of WZ-ZnSe:N are -2.35 and -2.62 respectively, with an about 17.17% deviation from their values in the ZB phase. And the new non-diagonal components for $Z(Zn)^*$ and $Z(Se)^*$ are negligibly small.

C. Strain effect on optical phonon frequencies

To understand the strain effect in different ZnSe materials, we calculated further the phonon frequencies of ZB and WZ structures with variant lattice constants. For the isotropic ZB structure, its strain tensor is diagonal, as $\xi_{ZB} = \begin{pmatrix} \delta & 0 & 0 \\ 0 & \delta & 0 \\ 0 & 0 & \delta \end{pmatrix}$, where δ is variable between -1.6% and 1.6% with a step of 0.2%. Note that the compressive strains are signed negative and the tensile ones are positive. For the WZ case, its strain tensor with the symmetry can be taken as $\xi_{WZ} = \begin{pmatrix} \delta_1 & 0 & 0 \\ 0 & \delta_1 & 0 \\ 0 & 0 & \delta_2 \end{pmatrix}$, where δ_1 is within the *ab* plane and δ_2 is along the *c* axis of the WZ unit cell.

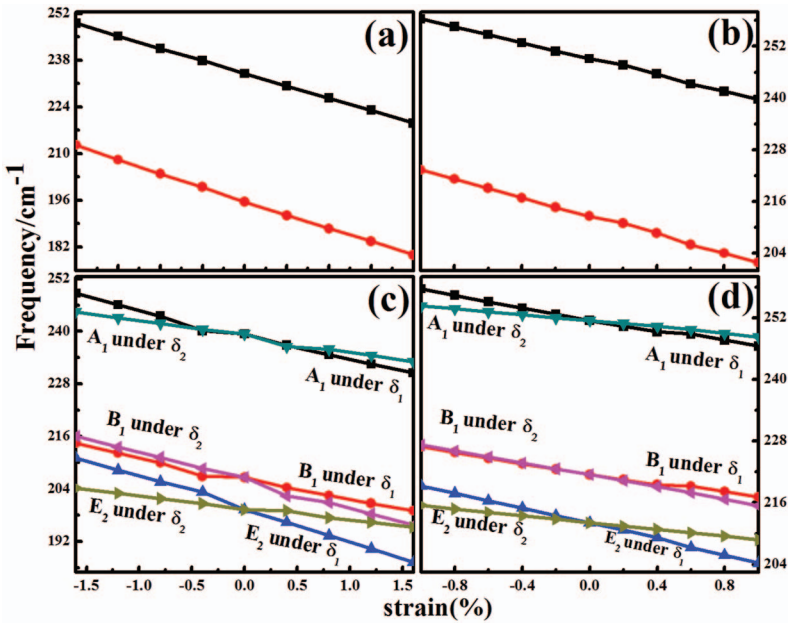

FIG. 3. Strain-dependent optical phonon frequencies of ZB ZnSe on (a) theoretical and (b) experimental lattice parameters; Strain-dependent optical phonon frequencies of WZ ZnSe on (c) theoretical and (d) experimental lattice parameters.

The calculated strain-dependent optical phonon frequencies of ZB ZnSe starting from their theoretical and experimental lattice parameters are plotted in Fig. 3(a) and Fig. 3(b) respectively. These mode frequencies shows linear dependence on strain, with a slope of -9.34 ± 0.02 cm^{-1}/% for the LO mode and -10.39 ± 0.07 cm^{-1}/% for the TO modes. Such linear dependence of LO and TO modes with strain can be explained by their effective force constants as functions of bond length.[8] An approximate linear increase for the LO-TO splitting on strain can be deduced, which results from the interplay of macroscopic dielectric constant and Born effective charges.[8,34,35] The consistent monotonic enhancement of LO and TO modes has also been obtained experimentally by Green *et al*.[36] and theoretically by Saib *et al*.[24] and Basak *et al*.[37] Our calculations also demonstrate that the distinct component of Born effective charges, $Z(Zn/Se)_{xx}^*$, change linearly with strain with a very small slope in the absolute value of 0.05 cm^{-1}/%.

Unlike the ZB phonons, the strain dependence of the WZ ones is not exactly linear as shown in Fig. 3(c) and Fig. 3(d) with the theoretical and experimental lattice parameters as the zero-strain points respectively. Here we select three WZ phonon modes at Γ, namely A_1(LO), B_1 and E_2, to label the strain effect of WZ-ZnSe. If starting from the theoretical lattice constants, the frequencies of these optical modes versus strain show a kink around $|\delta_{1,2}| \geq 0.4$. For δ_1, the frequency change slopes before the kink are respectively -7.08 ± 0.32 cm^{-1}/%, -6.27 ± 0.34 cm^{-1}/% and -6.48 ± 0.22 cm^{-1}/% for A_1, B_1 and E_2 mode, and those after the kink are correspondingly -5.56 ± 0.16 cm^{-1}/%, -4.71 ± 0.17 cm^{-1}/% and -7.55 ± 0.04 cm^{-1}/%. For δ_2, the corresponding values are -3.17 ± 0.10 cm^{-1}/%, -5.96 ± 0.11 cm^{-1}/% and -3.01 ± 0.07 cm^{-1}/% before the kink and -2.92 ± 0.41*cm*$^{-1}$/%, -5.65 ± 0.42 cm^{-1}/% and -3.17 ± 0.21 cm^{-1}/% after the kink. Moreover, we find that the absolute values of the change slopes of Z_{zz}^* are smaller than Z_{xx}^* as the functions of δ_1, but larger than Z_{xx}^* as the functions of δ_2. The strain influences on the distinct component of Z^* are also tiny in the WZ structures, with the absolute slope values between 0.01 and 0.04 cm^{-1}/%. When the zero point of strain is defined at the experimental lattice parameters, all the considered phonon frequencies decrease linearly with strain except that a kink appears for A_1 and B_1 when $0.4\% < \delta_1 < 0.6\%$, as shown in Fig. 2(d). Before the kink, the slopes of A_1 and B_1 are -5.99 ± 0.06 cm^{-1}/% and -5.30 ± 0.05 cm^{-1}/% respectively, and they are -5.91 ± 0.04 cm^{-1}/% and -5.29 ± 0.02 cm^{-1}/% after the kink. No kink appears for those phonon frequencies under δ_2. The corresponding slopes of A_1 and B_1 frequencies versus δ_2 are -2.97 ± 0.04 cm^{-1}/% and -5.88 ± 0.04 cm^{-1}/%.

And the slopes of E_2 frequency are -7.48 ± 0.09 cm^{-1}/% and -3.31 ± 0.01 cm^{-1}/% under δ_1 and δ_2 respectively.

IV. CONCLUSIONS

In summary, using the DFPT method implemented in code VASP combined with code PHONOPY we have calculated the phonon dispersion curves of ZnSe in the ZB and WZ phases. The obtained phonon dispersion curves of ZB-ZnSe in this work agree well with the data available in the literature. Comparing the optical phonon modes of ZB and WZ phases, we suggest the characteristic E_2 modes at about 50 cm^{-1} and the E_1 and another E_2 modes around 200 cm^{-1} of WZ-ZnSe can be used to identify the WZ phase of ZnSe. Moreover, we find that substitutional N incorporation will introduce new optical phonons above 500 cm^{-1} in both phases, and the splitting of them is much larger in the WZ phase than that in ZB phase. The dependence of the frequency of the Γ-point optical phonons on the strain has also been determined, the results could be important parameters for the strain/stress measurement of strained ZnSe crystals with the spectroscopic methods.

ACKNOWLEDGMENTS

The authors acknowledge the support of the National Natural Science Foundation of China (No. 11174273).

[1] P. Y. Yu and M. Cardona, *Fundamentals of Semiconductors: Physics and Materials properties*, 3rd ed. (Springer, Berlin, Heidelberg and New York, 2005).
[2] D. L. Dreifus, B. P. Sneed, J. Ren, J. W. Cook Jr., J. F. Schetzina, and R. M. Kolbas, Appl. Phys. Lett. **57**, 1663 (1990).
[3] T. Yasuda, K. Kimura, S. Miwa, L. H. Kuo, C. G. Jin, K. Tanaka, and T. Yao, Phys. Rev. Lett. **77**, 326 (1996).
[4] X. W. Zhang, X. J. Zhang, L. Wang, Y. M. Wu, Y. Wang, P. Gao, Y. Y. Han, and J. Jie, Nanotechnology **24**, 395201 (2013).
[5] Y. Y. Lai, Y. P. Lan, and T. C. Lu, Light: Sci. Appl. **2**, e76 (2013).
[6] C.-Y. Yeh, S.-H. Wei, and A. Zunger, Phys. Rev.B **50**, 2715 (1994).
[7] B. Hennion, F. Moussa, G. Pepy, and K. Kunc, Phys. Lett. A **36**, 376 (1971).
[8] F. Cerdeira, C. J. Buchenauer, F. H. Pollak, and M. Cardona, Phys. Rev. B **5**, 580 (1972).
[9] A. Dal Corso, B. Stefano, and R. Resta, Phys. Rev.B **47**, 3588 (1993).
[10] A. V. Postnikov, O. Pagès, and J. Hugel, Phys. Rev. B **71**, 115206 (2005).
[11] R. K. Kremer, M. Cardona, R. Lauck, G. Siegle, and A. H. Romero, Phys. Rev. B **85**, 035208 (2012).
[12] Q. Su, L. J. Li, S. Y. Li, and H. P. Zhao, Mater. Lett **92**, 338 (2013).
[13] X. J. Zhang, D. D. Wang, M. Beres, L. Liu, Z. X. Ma, P. Y. Yu, and S. S. Mao, Appl. Phys. Lett. **103**, 082111 (2013).
[14] W. Lin, S. P. Guo, M. C. Tamargo, I. Kuskovsky, C. Tian, and G. F. Neumark, Appl. Phys. Lett. **76**, 2205 (2000).
[15] S.-I. Nakashima, A. Fujii, K. Mizoguchi, A. Mitsuishi, and K. Yoneda, Jpn. J. Appl. Phys. **27**, 1327 (1988).
[16] M. Grün, C. Klingshirn, A. Rosenauer, J. Zweck, and W. Gebhardt, Appl. Phys. Lett. **63**, 2947 (1993).
[17] J. F. Justo, M. De Koning, W. Cai, and V. V. Bulatov, Phys. Rev. Lett. **84**, 2172 (2000).
[18] L. Sugiura, J. Appl. Phys. **81**, 1633 (1997).
[19] S. Suzuki, Y. Kaifuchi, H. Kumada, Y. Ishitani, and A. Yoshikawa, phys. stat. sol. (b) **241**, 475 (2004).
[20] J. Hu, Y. Bando, J. H. Zhan, Z. W. Liu, D. Golberg, and S. P. Ringer, Adv.Mater. **17**, 975 (2005).
[21] C. X. Shan, Z. Liu, X. T. Zhang, C. C. Wong, and S. K. Hark, Nanotechnology **17**, 5561 (2006).
[22] H. T. Wang, T. Tian, S. C. Yan, N. P. Huang, and Z. D. Xiao, J. Cryst. Growth **311**, 3787 (2009).
[23] X. J. Zhang, D. D. Wang, M. Beres, L. Liu, Z. X. Ma, P. Y. Yu, and S. S. Mao, Appl. Phys. Lett. **103**, 082111 (2013).
[24] S. Saib, M. Ajmal Khan, and N. Bouarissa, Physica B **407**, 3570 (2012).
[25] L. Liu, K. L. Teo, Z. X. Shen, J. S. Sun, E. H. Ong, A. V. Kolobov, and Y. Maeda, Phys. Rev. B **69**, 125333 (2004).
[26] B. Stefano, S. De Gironcoli, and A. Dal Corso, Rev. Mod. Phys. **73**, 515 (2001).
[27] J. P. Perdew, K. Burke, and M. Ernzerhof, Phys. Rev. Lett. **77**, 3865 (1996).
[28] G. Kresse and J. Hafner, Phys. Rev. B **47**, 558 (1993).
[29] G. Kresse and J. Furthmüller, Comput. Mat. Sci. **6**, 15 (1996).
[30] G. Kresse and J. Furthmüller, Phys. Rev. B **54**, 11169 (1996).
[31] G. Kresse and D. Joubert, Phys. Rev. B **59**, 1758 (1999).
[32] R. M. Pick, M. H. Cohen, and R. M. Martin, Phys. Rev.B **1**, 910 (1970).
[33] A. K. Arora, E.-K. Suh, U. Debska, and A. K. Ramdas, Phys. Rev.B **37**, 2927 (1988).
[34] A. R. Goñi, H. Siegle, K. Syassen, C. Thomsen, and J.-M. Wagner, Phys. Rev. B **64**, 035205 (2001).
[35] X. Gonze and C. Lee, Phys. Rev. B **55**, 10355 (1997).
[36] R. G. Greene, H. Luo, and A. L. Ruoff, J. Phys. Chem. Solids **56**, 521 (1995).
[37] T. Basak, M. N. Rao, M. K. Gupta, and S. L. Chaplot, J. Phys.: Condens. Matter **24**, 115401 (2012).